

Electron Transfer in Solid-State Materials: Photodynamic Fluorescence Diagnostics Using Energy Level Diagrams II

*S. H. Ehrlich
12 Courtenay Circle
Pittsford, New York/USA*

Abstract

This paper has related silver halide (AgBr, AgCl, β AgI) band gap energies to the common reference vacuum level and also the standard potential for redox couples referenced to the normal hydrogen electrode. This relationship suggests the thermodynamic limitations for photoreactions that can be carried out with charge carriers in the photographic silver halide microcrystals, dyes and other semiconductor materials of known band gap values. The author has not calculated mean field interactions such as the various aspects of intercalation or interaction energies that a given ion would feel if adjacent sites were full. Iridium III, rhodium III complexes, and iodide energies from literature values are reasonably placed within the band gap of AgBr in order to support the understanding of photophysical electron transfer within heterogeneous, two-phased photosensitive systems and other imaging systems. The known band gap relationships allow design and synthesis of fluorescent probes or sensors to produce consistent models of complex medical or biological processes.

Introduction

In general, an electron transfer may occur between a semiconductor electrode and a donor or an acceptor in solution. The more specific case at hand is the photoexcitation of a silver halide microcrystallite and the transfer of the electron from the solid phase, the electrode, which serves as an electron sink or source. Alternatively, the redox reaction could take place at the interface of the nanoheterogeneous system or quantum cluster. The solid-state properties of these imbedded aggregates depend strongly on the cluster size and on the environment immediately surrounding these clusters; i.e., intercalation and mean field expressions for short-range crystal lattice. The charge at the interfaces controls the thermodynamics and kinetics of the heterogeneous redox reactions. The electrical field due to these charges at the interface is the major difference with respect to homogenous analogues. The photoexcitation with ensembles of relatively small

numbers often fail to statistically represent all the host aggregates that may remain isolated with respect to the reaction time scale; thus, a variation of activation energies. Another interesting feature of these heterogeneous systems is the localization or position restriction of the epitaxial clusters in or upon the surface of the host crystal; e.g., faces, corners or edges of the crystals.

This paper describes an attempt to assemble a large quantity of data and present some possible correlation with several potential photographic imaging systems and potential applications for design of sensors and fluorescence medical diagnostics.

Discussion and Results

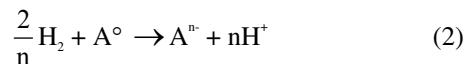
Electrode Potential Relationship with Inorganic Materials.

The discussion centers on the Fermi level of a redox electrolyte expressed in terms of electrochemical potentials under standard conditions and the relation

$$E_f^\circ(\text{redox}) = \mu_{A^{n-}}^\circ - \mu_A^\circ - nF\phi_{\text{solution}} \quad (1)$$

(ϕ , Galvani potential)

to the standard redox potential of the A°/A^{n-} redox couple. The normal hydrogen electrode (NHE) in electrochemistry is used as a reference. The Gibbs free energy $\Delta G_{\text{NHE}}^\circ$ of the solution reaction describes the redox potential $E_{\text{NHE}}^\circ(A^\circ/A^{n-})$ or



under standard conditions, where

$$\Delta G_{\text{NHE}}^\circ = -nFE_{\text{NHE}}^\circ \quad (3)$$

The vacuum or absolute potential scale is sometimes utilized instead of expressing redox potentials with respect to the NHE. In the former case, the equilibrium



where

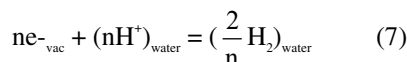
$$\Delta G_{\text{vac}}^\circ = \mu_{A^{n-}}^\circ - \mu_A^\circ = -nFE_{\text{vac}}^\circ \quad (5)$$

assuming the chemical potential of the electron at rest in vacuum, at infinite distance from the electrodes is zero. Comparisons of Eqs. 1 and 5 yields

$$E_f^\circ(\text{redox}) = -nFE_{\text{vac}}^\circ - nF\phi_{\text{solution}} \quad (6)$$

which shows the Fermi level of the electron in solution is not identical with the redox potential expressed on the vacuum scale. In the field of photoelectrochemistry, it is frequently asserted that these quantities are identical.¹ Bockris and Khan² pointed out that only in the unlikely case where the inner solution potential, Galvani potential, is zero does the condition $E_f^\circ(\text{redox}) = -nFE$ hold, as shown in Eq. 6.

Relating E_{vac}° to E_{NHE}° is accomplished by adding Eq. 7 to



Eq. 2 and obtaining Eq. 4 for which the standard free energy is known to be $-n(4.5 \pm 0.3)\text{eV}$.³ In order to convert a redox potential measured against the normal hydrogen electrode (NHE) to that expressed on the vacuum scale, the following relation is given, Eq. 8. A recent series of papers discussing conversion of

$$E_{\text{vac}}^\circ = E_{\text{NHE}}^\circ + 4.5 \quad (8)$$

relative to absolute potentials are listed.⁴⁻⁶

The increasing order of positive potentials beginning with 0.0 and ending with +5.5 V describes the ease of reduction; whereas the reduction reactions having reduction potentials more negative than that of the standard hydrogen electrode, beginning with 0.0 and ending with -1.5 V, describe the increasing difficulty of reduction. The standard electrode potential of an electrode reaction $E^\circ(M^{n+}/M^\circ)$ is the standard potential of a reaction in a cell whose left-hand electrode is a hydrogen electrode (IUPAC) convention. The convention is noted by $E^\circ(S/S^2) = -0.47627\text{ V}$ or $E^\circ(S_n^{2+}/Sn) = -0.1364\text{ V}$ with the temperature at 298.15 K under standard conditions of concentration; e.g., C° is 1 mol L^{-1} , $C^\circ \rightarrow 0$ and $a_A^\circ = 1$.

The energy levels for the conduction bands of AgBr, AgCl, and βAgI are 4.57, 4.59 (3% iodide), 4.51, and 3.90 eV, whereas the valence level measurements for AgBr, AgBr_{97.3}, AgBr_{74.26}, AgCl, AgI indicate 7.14, 7.04 (3% iodide), 6.90 (26% iodide), 7.55, and 6.60 eV, respectively (Figures 1 and 2)^{7,8a} (dashed lines). Normal hydrogen

electrode potentials have been taken from the literature.^{8b} However, solid-state analysis and photographic sensitization experiments (solid lines) have yielded 3.30, 3.30, and 3.90 eV for conduction band determinations. The valence energy levels for the earliest measurements were taken to be 5.87, 6.50, and 6.75 eV, respectively. The band gap for several semiconductors have also been taken from the literature.^{8c,d} But using the values published by Tejada et al.⁹ (AgCl 3.1 eV, AgI 3.7 eV) reverses the relative positions of the conduction bands of the first mentioned data of Bauer and Spicer.⁷

The solid-state properties of imbedded aggregates depend strongly on the cluster size and the environment immediately surrounding these clusters and may be described by terms within an overlap wavefunction model of the holes and electrons between different atoms or ions,¹⁰⁻¹⁷

$$E_g(R) = E_g(R=00) +$$

$$\frac{h^2}{2} \frac{\Pi^2}{R^2} \left[\frac{1}{m_{e^-}^*} + \frac{1}{m_{h^+}^*} \right] - \frac{1.8e^2}{\epsilon R} + \frac{e^2}{R} \sum_{n=1}^{\infty} \alpha_n \left(\frac{S}{R} \right)^{2n} \quad (9)$$

Figure 1 shows the energy of the lowest excited electronic state (i.e., the conduction band plus the transition recombination energy at the peak photoluminescence wavelength) versus the small iodide cluster diameter (R). The optical frequency dielectric for AgI (486 nm), $\epsilon = 5.419$, is inserted in the Coulomb attraction term and the third solvation energy loss term is not applicable. The effective masses $m_{e^-}^*$, $m_{h^+}^*$ of electrons and holes are approximated from literature values by comparing semiconductor properties. Silver bromide effective masses have been used as a reference. In general, it is shown that the smaller the cluster size, the greater the band state; the wider the band, the smaller the effective mass.

Figures 2 and 3 show band edge positions of semiconductors^{8c,d} with respect to AgBr, AgCl, and βAgI . The positions are given both as potentials^{8a,b} versus NHE and as energies versus the electron in vacuum. The dashed lines are of data from different analytical procedures in comparison to the solid lines as noted previously.

Figures 4-12 are graphic interpretations of band positions of AgBr, AgBr, I, AgCl, and βAgI with respect to NHE potentials^{8a,b} and as energies versus the electron in vacuum. The band gap positions are also related to redox couples in aqueous solutions.¹⁸ The dopants are hexagonal configurations that are substituted into the crystal lattice with a common anion sublattice. The reduction by the photoexcited conduction band electron can take place when the redox couple lies below the bottom of the silver halide conduction band edges; and oxidation occurs by a valence band hole when the couple lies above the top of the valence

band edge. Likewise, each of the semiconductors (Figures 2 and 3) is subject to the photo-oxidation and reduction processes similar to the silver halide materials in order to present new imaging systems.

The experimental data of I^{n-} , A-H solid lines describes the AgBr, I cryogenic photoluminescence involving I^{n-} in the region ~500 nm to 620 nm originating from the conduction band position of 3.30 eV.¹³ The dashed lines represent conduction energy band reference levels for the recombination emission to the iodide cluster centers (also dashed lines A-H). Recently, Ehrlich has related an iodide shallow electron trapping center, 0.065 eV, beneath the conduction band of AgBr, I microcrystallites by activation energy determination from low-temperature photoluminescence measurements.¹⁶ Also noted¹⁷ within the AgCl, I^{n-} clusters were the recombination photoluminescence emissions of several complexes between 5.63 and 5.72 eV. Multitudes of redox couples are available within this range as seen in column Iⁿ⁻ #31.

Dyes Adsorbed to AgX Surfaces²¹⁻²⁹ and the Inter-relation with Semiconductors.

The positioning of the energy levels of dyes relative to the silver halide band gap is related to the lowest vacant energy level of the ground state dye molecule (E_{LV}) of polarographic reduction potential (ER) and the highest occupied energy level (EHO) as related to the polarographic oxidation potential (EOX) and not the long-wavelength maximum. Hence, the dyes relate to the silver halide energy levels, and the silver halide relates to the bulk of the semiconductor literature with dopant and chemical sensitizers, therefore, each system can be related to each other via their energy levels.

Nanoscale Photodynamic Fluorescence Techniques.

Use of nanoparticles – quantum clusters – quantum dots – could make diagnoses of bacteria, viruses, and cancer markers possible and widely accessible.

The clear and narrow emission profiles of quantum dots allow multiplexed fluorescence imaging and may be useful for medical imaging. The chip may be temperature controlled, using a Peltier element, optical excitation, and a detection system.

The real-time nucleic acid sequence-based amplification (NASBA), a technique used to rapidly copy RNA on etched silicon bonded to glass, excited at 494 nm and detected at 525 nm, is a reality.³⁰ (A protein laboratory on a chip.)

Porphyryns have potent cancer-destroying properties; they accumulate selectively in cancer cells and are activated by red light; however, potency, selectivity, and residency within the body could be adjusted by coupling with a semiconductor capable of receiving the excited electron to its conduction band, and the production of oxygen-free radicals, which destroy tumors. The first photosensitizing drug to fulfill the stringent criteria without causing photosensitivity, is Verteporfin, a synthetic porphyrin, used not to treat cancer, but to prevent age-related macular

degeneration (AMD – blindness by accumulation of the blood vessels growing under the retina). With activation by red laser light, the verteporfin seals off the vessels, sparing the overlying retina.³¹ By adjusting the chemical aggregate cluster size, the efficiency of electron transport may be adjusted.

Initial Tumor Growth Model.

Fluorescence imaging probes for enzymes that promote cell growth can be utilized to follow the growth molecular mechanisms. Enzyme proteins, epidermal growth factors, needed for continual growth and division by a cancer cell as it ages are secreted into the blood or urine and probed by fluorescence sensors. Chemistry that prevents the production of these enzymes may control the tumor. The growth factors fit into sites, receptors (substrates) on the tumor cell's surface. The initial tumor growth model relates drug chemistry with receptors (substrates). A model of catalysis involving only one substrate and not involving chain reactions is the following:



where C is the enzyme, S is the substrate/receptor, X is the intermediate adsorption complex/cancer growth, Y is the additional chemistry formed, and k_1 and k_{-1} are rate constants, and



where W is the molecule that reacts with X, P is the product of cancer formed, Z is the elimination of the molecule from P, and k_2 is a rate constant.

Equilibrium Treatment

$$\frac{[X][Y]}{[C][S]} = \frac{k_1}{k_{-1}} = K \quad (12)$$

where

$$[C] = [C_0] - [X], [S] = [S_0] - [X] \quad (13)$$

Equation (12) becomes:

$$\frac{[X][Y]}{([C_0] - [X])([S_0] - [X])} = K \quad (14)$$

Two special cases exit:

Case 1. $[S_0] \gg [C_0]$, (15)

therefore,

$$[S_o] - [X] \approx [S_o] \quad (16)$$

$$\frac{[X][Y]}{([C_o] - [X])[S_o]} = K \quad (17)$$

$$[X] = \frac{K[C_o][S_o]}{K[S_o] + [Y]} \quad (18)$$

The rate of reaction is, therefore:

$$\frac{dS}{dt} = k_2[X][W] = \frac{k_2K[C_o][S_o][W]}{K[S_o] + [Y]} \quad (19)$$

when $K[S_o] < [Y]$, the rate varies linearly with $[S_o]$

when $K[S_o] > [Y]$, the rate is independent of $[S_o]$

when $[S_o] \gg [C_o]$, the rate varies linearly with $[C_o]$

Case 2. $[Co] \gg [So]$, $[Cop] = [Co] - [X]$ in Eq. (14),

which becomes

$$\frac{[X][Y]}{[C_o]([S_o] - [X])} = K \quad (20)$$

The rate of reaction is, therefore,

$$\frac{-dS}{dt} = \frac{k_2K[C_o][S_o][W]}{K[C_o] + [Y]} \quad (21)$$

Steady-State Treatment (when k_2 occurs rapidly)

$$\frac{dX}{dt} = k_1[C][S] - k_{-1}[X][Y] - k_2[X][Y] = 0 \quad (22)$$

Substitute $[Co] - [X] = [C]$, $[So] - [X] = S$

Therefore,

$$k_1([C_o] - [X])([S_o] - [X]) - k_{-1}[X][Y] - k_2[X][Y] = 0 \quad (23)$$

when $[X]$ is small, $[X]^2$ is neglected, then

$$X = \frac{k_1[C_o][S_o]}{k_1[Co] + k_1[S_o] + k_{-1}[Y] + k_2[W]} \quad (24)$$

the reaction rate is:

$$\frac{dS}{dt} = k_2[X][W] = \frac{k_1k_2[Co][So][W]}{k_1([C_o] + [S_o]) + k_{-1}[Y] + k_2[W]} \quad (25)$$

At low $[C_o]$ and $[S_o]$, the rate varies linearly with $[C_o]$ and $[S_o]$, and at high $[C_o]$ and $[S_o]$, the rate becomes independent of that concentration.

Conclusions

1. The author has related silver halide band gap energies to the common reference vacuum level and also indicated the standard potential for redox couples referenced to the normal hydrogen electrode. This relationship suggests the thermodynamic limitations for photoreactions that can be carried out with charge carriers in the photographic silver halide microcrystals and other semiconductor materials of known band gap values.

2. If reduction of a chemical species, quantum cluster, nanocluster, or aggregate in or on the silver halide host is to be reduced, the conductive band position of the silver halide (which is photoexcited) must be positioned above the relevant redox level to form a metastable state with the silver halide defect lattice.

3. Development of the silver-complex latent image may be internal to the grain or upon the surface at the interface of the aggregate or cluster.

4. The lowest unoccupied molecular orbital (LUMO) of the photon-absorbing adsorbed species cluster, or core semiconductor shelled or epitaxially placed upon silver halide, must be energetically positioned above the conduction band of the silver halide for photocatalysis of silver halide to occur.

5. Oxidation by a valence band silver halide hole occurs when the nonexcited couple (HOMO) highest occupied molecular orbital or semiconductor valence band lies above the photoexcited silver halide valence band.

6. Literature values (ESR) of shallow electron traps 0.446, 0.420, and 0.460 eV¹⁹ of iridium III hexachloride under the conduction band (also 0.2 eV (TSC) beneath the conduction band²⁰) would not distinguish the validity of the band gap measurements due to the activation energy reference to the conduction band. An activation energy also determined the positioning of the shallow trap at an emitting iodide center, 0.065 eV beneath the AgBr conduction band.

7. $Rh(CN)_6^{3-}/Rh(CN)_6^{4-}$ ($E^\circ = 0.9$ V) show deeper electron trapping than experimental iridium III hexachloride, which correlated with photographic results. Also, sulfide and iodide nanoclusters, and osmium complexes show photoluminescence quenching by electron trapping which correlated with the proposed energy diagrams of the silver halide systems.

8. IRM+, RhM+, RuM+, ReM+, OsM+ complexes (M3+X6-)3- have band gap positions related to redox couples in aqueous solutions. As a result of the octahedral

configuration, Oh symmetry, the electrode surface has the same stereo configuration within the AgX common anion sublattice: the more generalized position of energy levels using redox potentials are to be cautioned.

9. Energy level relationships are necessary to design sensors and imaging systems. Fluorescence diagnostics depend upon the following: 1) the electron transfer from the excited state or conduction band of a photon-absorbing entity to the ground state or valence band, 2) the transfer of the electron in the excited state to a semiconductor with subsequent emission, and the decreased efficiency of the electron transfer by quenching mechanisms.

10. Fluorescence imaging probes for enzymes that promote cancer cell growth can be utilized to follow the growth molecular mechanisms. The enzyme proteins, epidermal growth factors needed for continual growth by a cancer cell as it ages, are secreted into the blood or urine and probed by fluorescence sensors.

11. A model of growth catalysis by an enzyme and one substrate infer a competition for a receptor by the growth enzyme and a drug: 1) if the appropriate drug is adsorbed on the receptor of the tumor, the tumor will be terminal, and 2) if the growth enzyme is adsorbed on the receptor or interacts with the competing drug, the cancer will continue to grow.

References

1. R. Meming, *Electroanalytical Chemistry*, Vol. 11, A. J. Bard, Ed., Marcel Dekker, New York, 1979.
2. J. O. M. Bockris and S. U. M. Khan, *J. Phys. Chem.*, 87, 2599 (1983).
3. F. Lohman, *Z. Naturforsch., Teil A*, 22, 813 (1956).
4. R. Gomer and G. Tryson, *J. Chem. Phys.*, 66, 4413 (1977).
5. S. Trasatti, *J. Electroanal. Chem.*, 139, 1 (1982).
6. S. Trasatti, *J. Electroanal. Chem.*, 209, 417 (1986).
7. R. S. Bauer and W. E. Spicer, *Phys. Rev. Lett.*, 25, 1283 (1970); R. S. Bauer and W. E. Spicer, *Phys. Rev. B*, 14, 4539 (1976); R. S. Bauer, Ph.D. Thesis, Stanford University, 1970.
8. A. J. Bard, *Integrated Chemical Systems: A Chemical Approach to Nanotechnology*, John Wiley and Sons, New York, 1994. (b) A. J. Bard, R. Parsons, and J. Jordon, *Standard Potentials in Aqueous Solutions*, Marcel Dekker, Inc., New York, 1985; (c) N. Serpone and E. Pelizzette, *Photocatalysis, Fundamentals and Applications*, John Wiley and Sons, New York, 1989; (d) M. Grätzel, *Heterogeneous Photochemical Electron Transfer*, CRC Press, Boca Raton, FL, 1988.
9. J. Tejada, N. J. Shevchik, W. Braun, A. Goldman, and M. Cardona, *Phys. Rev. B*, 12, 1557 (1975).
10. L. E. Brus, *J. Phys. Chem.*, 80, 4403 (1984); *ibid* 79, 5566 (1983).
11. L. E. Brus, *J. Phys. Chem.*, 90, 2555 (1986).
12. L. E. Brus, *J. Quantum Electron*, 22, 1909 (1986).
13. S. H. Ehrlich, *J. Imaging Sci. Technol.*, 37, 73 (1993).
14. S. H. Ehrlich, *J. Imaging Sci. Technol.*, 38, 201 (1994).
15. S. H. Ehrlich, *J. Imaging Sci. Technol.*, 39, 97 (1995).
16. S. H. Ehrlich, *J. Imaging Sci. Technol.*, 41, 13 (1997).
17. S. H. Ehrlich and J. Edwards, *J. Imaging Sci. Technol.*, 43, 15 (1999).
18. D. R. Lide, Ed., *CRC Handbook of Chemistry and Physics*, 74th Edition, CRC Press, Boca Raton, FL, 1993-1994, pp. 8-21 to 8-31.
19. R. S. Eachus and M. T. Olm, *Cryst. Lattice Defects Amorphous Mater.*, 18, 297 (1989).
20. L. M. Kellogg, unpublished data, Eastman Kodak Company.
21. S. H. Ehrlich, *Photogr. Sci. Eng.* 18:179 (1974); *Photochem* 3:403 (1974) 75; *J. Phys. Chem.* 79:2228, 2234 (1975), *Photogr. Sci. Eng.* 20:5 (1976); *Photogr. Sci. Eng.* 23:348 (1979), *J. Imaging Sci. Technol.* 39:97 (1995).
22. S. H. Ehrlich and I. Leubner, *J. Imaging Sci. Technol.* 36:105 (1992).
23. J. Lenhard, *J. Imaging Sci. Technol.* 30:27 (1986).
24. Leubner, *Photogr. Sci. Eng.* 18:175 (1974), *Photogr. Sci. Eng.* 20:81 (1976), *Photogr. Sci. Eng.* 22:271 (1998).
25. T. L. Penner and P. B. Gilman, Jr., *Photogr. Sci. Eng.* 19: 102, (1975), *Photogr. Sci. Eng.* 20:97 (1976).
26. P. B. Gilman, R., *Photogr. Sci. Eng.* 18:418, 475 (1974), : *Photogr. Sci. Eng.* 19:207 (1975), *Photogr. Sci. Eng.* 28:226 (1984).
27. L. F. Costa and P. B. Gilman, Jr., *Photogr. Sci. Eng.* 18:261 (1974), *Photogr. Sci. Eng.* 19:207 (1975).
28. T. Tani, *Photogr. Sci. Eng.* 13:231 (1969); *Photogr. Sci. Eng.* 14:63 (1970), *Photogr. Sci. Eng.* 14:72 (1968);
29. T. Tani and S. Kikuchi, *Photogr. Sci. Eng.* 11:129 (1967); (b) T. Tani and S. Kikuchi, *Kogyo Kagaku Zasshi* 71 (1968); (c) T. Tani and S. Kikuchi, *Photogr. Sci. Eng.* 12:80 (1968); (d) T. Tani, K. Honda, and S. Kikuchi, *J. Electrochem. Soc. Japan* 37:17 (1969).
30. Gulliksen, *Analytical Chemistry*, Jan. 1, 9-14 (2004).
31. M. S. Blumenkranz et al., *Archives of Ophthalmology* 120:1307-1317 (2002).

Biography

Dr. Sanford H. Ehrlich received his BS in biology and chemistry from New York University and his MS in theoretical electrochemistry in 1957 from the same university, after his service in Korea. His research for his doctoral thesis was in the area of molecular surface spectroscopy investigating adsorption phenomena of polyelectrolytes. He received his PhD in 1962 from Adelphi and New York Universities. From 1963-1965 he carried out conductivity studies in materials at cryogenic temperatures at Air Products Co., PA. 1963-1967, as a senior researcher at the American Optical Co., MA, he investigated and invented variable transmission glasses via studying defect properties of glass. In 1967, he joined Eastman Kodak Company's Research & Development Laboratories. From 1967-1972, he investigated the sensitization and electron transfer properties in electrophotographic systems. Non-light-sensitive direct X-ray imaging systems were of interest. From 1972-1979, his efforts were directed to electron transfer processes involving spectral, chemical, and dopant sensitization of silver halides, using pulsed radiation transient spectroscopy. During this period, he invented surface coatings for finish glass lens molding and new aspherical pre-form glass processes for

molding lenses. Since 1979, he has developed novel techniques in laser microwave photoconductivity and fluorescence to investigate electron trapping in the solid state. He has applied these technologies to mechanistic studies relating to imaging processes in silver halide and other systems. He has been involved in chemiluminescent systems for diagnostic biochemistry. The most recent studies involve spectroscopic low-temperature photoluminescent investigations with quantum-sized clusters of iodide, silver, and silver sulfides in silver halide systems; also, kinetic processes of formation and electron-trapping efficiencies of quantum-sized silver halide clusters in gelatin matrices using stopped-flow and sequential techniques.

Dr. Ehrlich has also taught advanced courses in physics/biophysics, physical-, photo-, inorganic-, organic- and biochemistry at the University of Rochester and the

Rochester Institute of Technology over a period of 25 years. In May 1993, he was selected as a Fellow of the Society for Imaging Science and Technology. The award was in recognition of fundamental work toward understanding of the mechanisms of dopants and dye sensitization of silver halides. He also received the Journal Award (Science) for outstanding contributions in the area of basic sciences for the scientific paper entitled, "Spectroscopic Studies of AgBr with Quantum-sized Clusters of Iodide, Silver, and Silver Sulfides," in 1994. In 1998, Dr. Ehrlich was awarded the prestigious Lieven Gevaert Medal for his many contributions in spectroscopic analysis of silver halide and related imaging processes. This award is sponsored by Bayer Corporation/Agfa Division, which recognizes outstanding contributions in the field of silver halide photography.